JACS
JOURNAL OF THE AMERICAN CHEMICAL SOCIETY

Article

pubs.acs.org/JACS

# Enhanced Photovoltaic Performance of $CH_3NH_3PbI_3$ Perovskite Solar Cells through Interfacial Engineering Using Self-Assembling Monolayer

Lijian Zuo, Zhuowei Gu, Tao Ye, Weifei Fu, Gang Wu, Hanying Li,* and Hongzheng Chen*

State Key Laboratory of Silicon Materials, MOE Key Laboratory of Macromolecular Synthesis and Functionalization, Department of Polymer Science & Engineering, Zhejiang University, Hangzhou 310027, China

Supporting Information

**ABSTRACT:** Morphology control is critical to achieve high efficiency $CH_3NH_3PbI_3$ perovskite solar cells (PSC). The surface properties of the substrates on which crystalline perovskite thin films form are expected to affect greatly the crystallization and, thus, the resulting morphology. However, this topic is seldom examined in PSC. Here we developed a facile but efficient method of modifying the ZnO-coated substrates with 3-aminopropanioc acid ($C_3$-SAM) to direct the crystalline evolution and achieve the optimal morphology of $CH_3NH_3PbI_3$ perovskite film. With incorporation of the $C_3$-SAM, highly crystalline $CH_3NH_3PbI_3$ films were formed with reduced pin-holes and trap states density. In addition, the work function of the cathode was better aligned with the conduction band minimum of perovskite for efficient charge extraction and electronic coupling. As a result, the PSC performance remarkably increased from 9.81(±0.99)% (best 11.96%) to 14.25(±0.61)% (best 15.67%). We stress the importance of morphology control through substrate surface modification to obtain the optimal morphology and device performance of PSC, which should generate an impact on developing highly efficient PSC and future commercialization.

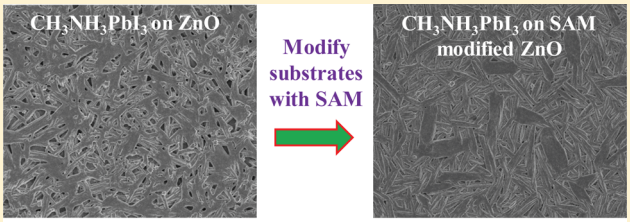


**SAM= 3-aminopropanioc acid. With deposition of SAM:**
1) Perovskite film crystallinity improved;
2) Pin-holes and charge traps reduced;
3) Perovskite solar cell efficiency enhanced by 31% (up to 15.67%).

## INTRODUCTION

The recent advent of perovskite solar cells (PSC) has encouraged the world's ambition toward the solar energy utilization due to the surge in device performance,[1−5] which came to a certified power conversion efficiency (PCE) of 17.9% within a quite short period.[6,7] Also, the PSC takes the advantages of low cost, light weight, flexibility, and roll-to-roll processing compatibility[8−11] over the silicon counterpart. These merits make it more competitive for future commercialization. To achieve high device performance, morphology control is critically important especially for the planar junction PSC, where the crystalline film of perovskite has to be self-standing without the support of a mesoporous scaffold.[4,12,13] The ideal morphology of planar junction PSC requires a homogeneous and highly crystalline film.[2,4,8,9,14−20] However, controlling the morphology of perovskite film remains a critical challenge due to the complex crystal growth process of the perovskite. Generally, the "island" like structures with poor crystallinity were obtained, leading to current leaking and negative influence on the charge dynamics of PSC.[12,21,22] Therefore, efforts have been made for morphology control through modification of the perovskite crystallization kinetics.

To date, the processing of perovskite thin films includes the one-step solution processing,[7,23] two-step sequential deposition method,[8,24,25] and the vacuum evaporation deposition.[12,13] The essence of morphology control protocols developed in context of these processing methods focuses on the delicate control of the crystallization kinetics,[26,27] e.g. adding additives,[28,29] varying the composition,[30] solvent washing,[31] and controlling annealing time, temperature, or atmosphere,[14,32,33] etc. Considering that perovskite thin films are prepared on substrates during the device fabrication, the surface properties of the substrates are expected to greatly affect the crystallization of perovskite. Generally, good wetting property of the substrate is required to achieve the homogeneous crystalline structure.[34] For the $CH_3NH_3PbI_3$ perovskite film, the substrates covered with amino or ammonium group would favor the growth of smooth and high crystalline perovskite films. A simple method to obtain the amino rich surface is to modify the substrate with self-assembling monolayers (SAM) that contain amino terminal groups.[34] However, this topic is rarely explored for planar junction PSC.

In addition to the morphology control, the delicate interfacial modification is strictly required to achieve better energy level alignment at the interface as well for highly efficient planar junction PSC.[10−13] At the cathode side, electron extraction is realized by using an electron selective transporting layer (ETL), e.g. $TiO_2$,[2,12] ZnO,[8] CdSe,[35] or perylene-diimide.[36] Most recently, further lowering the work function of the ETL to

**Received:** December 9, 2014
**Published:** February 4, 2015




DOI: 10.1021/ja512518r
J. Am. Chem. Soc. 2015, 137, 2674−2679

better align with the conduction band minimum (CBM) for the $CH_3NH_3PbI_3$ (−3.75 eV) was demonstrated to improve the PSC device to a record value of 19.3%.[16] To lower the electrode work function, the SAM strategy was also demonstrated effective due to the formation of permanent dipole moments.[37]

In this work, we demonstrated that the deposition of 3-aminopropanoic acid SAM ($C_3$-SAM) onto the sol−gel ZnO (defined as ZnO in the following) layers would induce significant improvement in the morphology of $CH_3NH_3PbI_3$ perovskite film due to the enhanced wetting between the ZnO and perovskite. In addition, the interfacial energy level alignment was also improved owing to the formation of permanent dipole moment. As a result, a decent improvement in device performance of $CH_3NH_3PbI_3$ PSC (Device structure shown in Figure 1) was observed with the device PCE surging from 11.96% (best) to 15.67% (best). We stress the importance of substrate surface properties for perovskite morphology control and device optimization. Due to the simplicity and efficacy, this strategy should generate an impact on developing high efficient PSC for future commercialization.

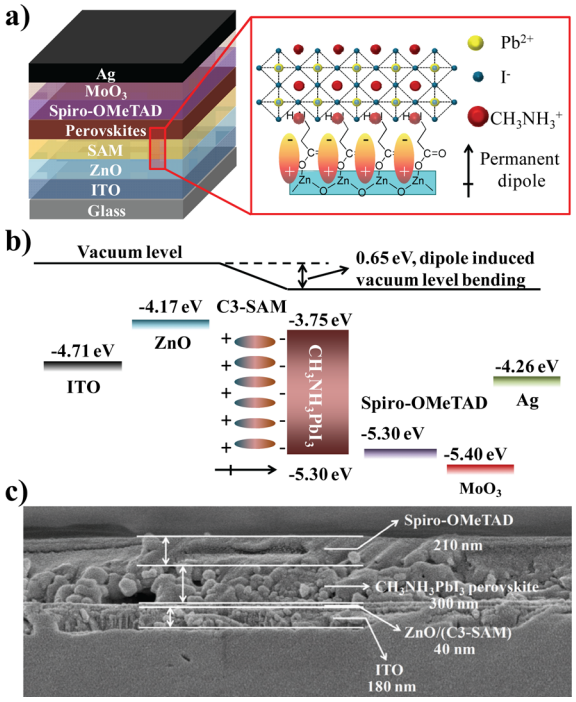


**Figure 1.** (a) Schematic diagram of perovskite solar cell device structure, SAM induced permanent dipole formation, and involvement of the SAM in the crystalline structure of perovskite crystals. (b) Schematic energy level of each layer in perovskite solar cell. (c) Cross-section SEM image of the PSC device (without $MoO_3$/Ag).

## EXPERIMENTAL SECTION

**Materials and Equipment.** all of the materials were purchased from the Sigma-Aldrich Corp., if not specified. The Spiro-OMeTAD was from Lumi Tech. Corp. (Taiwan, China). The atomic force microscope (AFM) measurement was carried out on the Veeco Multimode scanning probe microscope (Veeco IIIa) in tapping mode. The X-ray diffraction patterns were recorded at a scan rate of 5 deg/min on the Rigaku D/max-2550PC X-ray diffractometer with Cu K$\alpha$ radiation (1.5406 nm). The UV−visible absorption spectra were measured on a Varian CARY100 Bio spectrophotometer. The SEM data were scanned by S-4800 (Hitachi) field-emission scanning electron microscope (FESEM). The PL spectra (both of steady state and transient spectra) are measured using an Edinburgh Instruments FLS920 spectrometer. The UPS measurement is carried out on an integrated ultrahigh vacuum system equipped with multitechnique surface analysis system (Thermo ESCALAB 250Xi) with the He (I) (21.2 eV) UV excitation source.

**Device Fabrication and Measurement.** The ITO coated substrates were cleaned sequentially in detergent, acetone, and isopropanol ultrasonic bath for 15 min, respectively. After cleaned by the UV-Ozone machine, 40 nm ZnO was deposited by spin-coating and annealed at 160 °C for 30 min in air. The preparation of ZnO precursor solution followed ref 17, where the $Zn(Ac)_2{\cdot}2H_2O$ was dissolved in 2-methoxyethanol and stabilized by monoethanolamine. The ZnO coated glass/ITO substrates were transferred into the glovebox for further deposition of $C_3$-SAM from the methanol solution (2 mg/mL). In the following, freshly prepared $CH_3NH_3PbI_3$ solution was spin-coated and annealed at 80 °C for 4 min to form an ∼350 nm perovskite layer. The solution of perovskite was prepared by mixing the pristine $PbI_2$ solution and $CH_3NH_3I$ solution of *N*,*N*-dimethylformamide (DMF). Lithium doped 2,2′,7,7′-tetrakis(*N*,*N*-di-4-methoxyphenylamino)-9,9′-spirobifluorene (spiro-OMeTAD)[38] was deposited from the solution of chlorobenzene by spin-coating. Finally the substrates were transferred into a vacuum chamber to deposit 10 nm $MoO_3$ and 100 nm Ag to finish the device fabrication process. The device area is defined around 5.2 $mm^2$ by the cross section of the electrodes. The *I*−*V* characteristic of PSC was recorded on the Keithley source unit under AM 1.5 G 1 sun intensity illumination by a solar simulator from Abet Corp. Notably, certain measurement errors were caused, including the device area error of 3%, light intensity error of 2%, and calibration error of 1%.

## RESULTS AND DISCUSSION

**Morphology Evolution.** Initially, we investigated the effect of SAM on the morphology of $CH_3NH_3PbI_3$ perovskite film grown via a one-step method. Panels a and b of Figure 2 show the surface morphology of perovskite films imaged by the AFM in tapping mode. As shown, the perovskite crystals on bare ZnO appeared like nanorods, with diameters of 200−300 nm

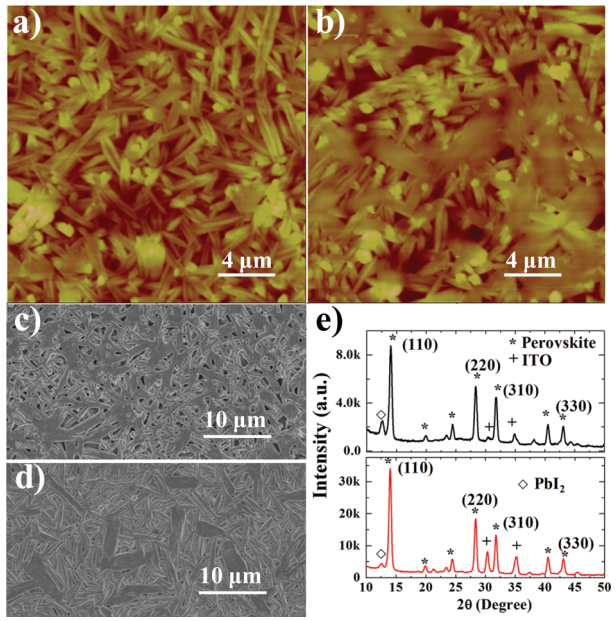


**Figure 2.** AFM images of $CH_3NH_3PbI_3$ perovskite on (a) bare ZnO and (b) ZnO/$C_3$-SAM. SEM images of $CH_3NH_3PbI_3$ perovskites on (c) bare ZnO and( d) ZnO/$C_3$-SAM. (e) XRD patterns of perovskite films on ZnO (black line) and ZnO/SAM substrates (red line).



DOI: 10.1021/ja512518r
J. Am. Chem. Soc. 2015, 137, 2674−2679

and a length of ~4 μm, similar to the literature reports.[29,39] These nanorods on bare ZnO presented a tilt conformation to the substrates with irregular directions, resulting in a quite rough surface with a high density of pin-holes. In contrast, with $C_3$-SAM modification, a considerable portion of the perovskite crystals was expressed in a more extending plate-like shape, with the lateral dimension up to several micrometers. Panels c and d of Figure 2 show the scanning electron microscope (SEM) images of perovskite film surface morphology on different substrates. Complementary to the AFM images, the SEM images of the $CH_3NH_3PbI_3$ film directly showed that the number of pin-holes was reduced with deposition of $C_3$-SAM on the ZnO.

Figure 2e shows the X-ray diffraction (XRD) patterns of $CH_3NH_3PbI_3$ films grown on ZnO with or without $C_3$-SAM. The peaks at 14.1°, 28.4°, and 42.1° could be attributed to the (110), (220), and (330) faces of $CH_3NH_3PbI_3$ perovskite crystalline structure, respectively.[7,12] It was observed that all these perovskite diffraction peaks became significantly enhanced with the insertion of SAM, indicative of the improvements in the crystalline property of the $CH_3NH_3PbI_3$ film.[28] Also, the AFM and SEM images indicate the enlarged crystalline domains in the lateral direction with the morphology evolution from rod-like to plate-like (Figure 2).

The morphology evolution of the perovskite film with deposition of $C_3$-SAM on ZnO could be attributed to the improved substrate miscibility with perovskite, where the amino group is expected to change into ammonium by hydrogen ion exchanging and involves into the crystalline structure of perovskite shown in Figure 1a. For highly efficient PSC, pin-holes free perovskite film with high crystalline properties are essentially important as shown in previous reports.[12,31] In this regard, this morphology evolution with $C_3$-SAM deposition might promise an improved device performance of PSC, which will be discussed below.

**PSC Device Performance.** To investigate the effect of SAM on the device performance, we fabricated PSC using ZnO as ETL with or without $C_3$-SAM modification based on the device structure illustrated in Figure 1a (glass/ITO/ZnO/($C_3$-SAM)/$CH_3NH_3PbI_3$/spiro-OMeTAD/$MoO_3$/Ag). The thickness of each layer is shown in Figure 1c. As shown in Figure 3

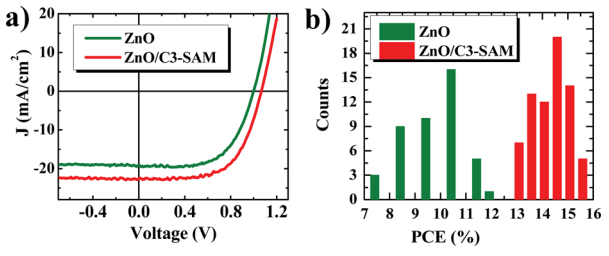


**Figure 3.** (a) *I*–*V* characteristics of $CH_3NH_3PbI_3$ PSC with the structure of glass/ITO/ZnO/($C_3$-SAM)/$CH_3NH_3PbI_3$/spiro-OMeTAD/$MoO_3$/Ag. (b) PCE histograms of $CH_3NH_3PbI_3$ PSCs with and without $C_3$-SAM on ZnO.

and Table 1, the PSC with bare ZnO as ETL showed the best PCE of 11.96%, which is similar to the literature report.[17] Remarkably, through deposition of $C_3$-SAM on ZnO, the best PCE surged to 15.67%, which stands as one of the highest values in the planar junction of PSC with ZnO as ETL. The introduction of the $C_3$-SAM resulted in an about 31% enhancement of PCE and simultaneous improvement of all

**Table 1. Device Parameters of PSC with or without $C_3$-SAM Modification**

| | | | | PCE(%) | |
|---|---|---|---|---|---|
| ETL | $V_{oc}$ (V) | $J_{sc}$ (mA/cm²) | FF (%) | averaged | best |
| ZnO | 0.99 | 19.12 | 0.63 | 9.81 | 11.96 |
| ZnO/$C_3$-SAM | 1.07 | 22.51 | 0.65 | 14.25 | 15.67 |

the device parameters, e.g. $J_{SC}$ increased from 19.12 to 22.51 mA/cm², $V_{OC}$ from 0.99 to 1.07 V, and FF from 0.63 to 0.65. In PSC, the device performance variation was typically observed from batch to batch, and here we fabricated nearly one hundred devices from more than ten batches to confirm the effect of $C_3$-SAM on the device performance. We found the PSC with bare ZnO as ETL showed a yield of 47%, while the yield increased to 70% with $C_3$-SAM modification. Figure 3b showed the statistic histogram of the device parameters. The device performance of PSC with $C_3$-SAM modification showed a narrowed distribution of PCE (range: 13.05% to 15.67%, with the averaged value of 14.25%). In comparison, without the $C_3$-SAM modification, much lower PCE (averaged value 9.81%) with a wide range (from 7.54% to 11.96%) was obtained. We attributed the improved reproducibility to the evolved morphology of $CH_3NH_3PbI_3$ film on the $C_3$-SAM surface. The improved device performance and better reproducibility unambiguously verified the significance of $C_3$-SAM on PSC optimization. The possible mechanisms for PSC performance enhancement are explored below.

**Enhanced Absorption.** In PSC, fully absorbing the solar irradiance is critical for high device performance. Here we found the improvements of the $CH_3NH_3PbI_3$ perovskite film morphology induced appreciable enhancement in its UV–visible absorption spectrum. As shown in Figure 4a, the absorption of $CH_3NH_3PbI_3$ perovskite film deposited on the $C_3$-SAM modified ZnO was significantly increased along the range of 450–790 nm, which was attributed to the more complete conversion of $PbI_2$ into $CH_3NH_3PbI_3$ perovskite, as

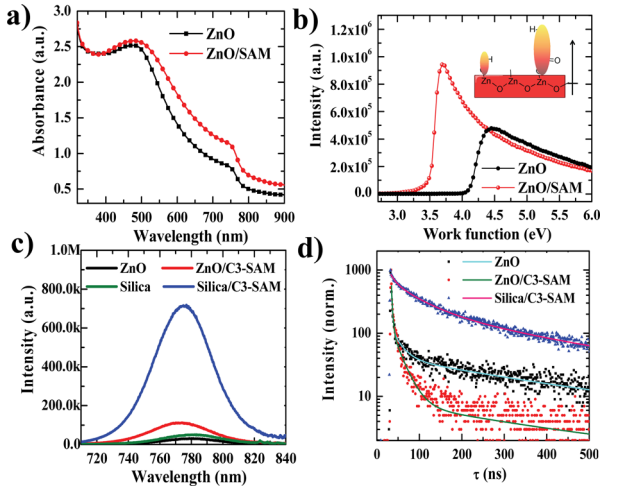


**Figure 4.** (a) UV–visible absorption spectra of perovskite films on ZnO with or without $C_3$-SAM modification, (b) ultraviolet photoelectron spectroscopy of bare ZnO and ZnO/$C_3$-SAM films, (c) steady state PL spectra of perovskite films on bare ZnO and silica with or without $C_3$-SAM modification, and (d) transient PL spectra of perovskite films on bare ZnO, ZnO/$C_3$-SAM, and silica/$C_3$-SAM substrates.



DOI: 10.1021/ja512518r
J. Am. Chem. Soc. 2015, 137, 2674–2679

Table 2. Transient PL Species of Perovskite on ZnO and $C_3$-SAM Modified ZnO

| | $\tau_1$ | | $\tau_2$ | | $\tau_3$ | |
|---|---|---|---|---|---|---|
| substrates | lifetime (ns) | content (%) | lifetime (ns) | content (%) | lifetime (ns) | content (%) |
| ZnO | 2.4 | 7.8 | 22.6 | 11.7 | 329.8 | 80.5 |
| ZnO/$C_3$-SAM | 2.0 | 21.0 | 12.6 | 62.8 | 148.4 | 16.2 |

demonstrated by XRD patterns (Figure 2e). Near the (110) peak of the perovskite film, a diffraction peak at 12.7° appeared, which was attributed to the (001) diffraction of $PbI_2$ crystals.[27] The existence of $PbI_2$ was reported to originate from the $CH_3NH_3PbI_3$ perovskite by release of the $CH_3NH_3I$ component during heating.[40,41] The excessive amount of $PbI_2$ in $CH_3NH_3PbI_3$ perovskite was expected to be detrimental to the device performance of PSC due to its electrical insulating property,[42] although a passivation effect was observed with a small amount of $PbI_2$ at the grain boundaries.[40] With deposition of the $C_3$-SAM, the intensity of this peak was significantly reduced, indicating the more complete conversion of $PbI_2$ into the $CH_3NH_3PbI_3$ perovskite structure. The subsequent enhancement in the absorption with deposition of $C_3$-SAM would contribute to the charge generation, which could be clearly seen in the EQE spectra (Figure S1, Supporting Information).

**Improved Energy Level Alignment.** Interfacial contact of PSC is critical for efficient charge extraction. For the cathode interface, lowered work function is favored due to the reduction in charge extraction barrier. The deposition of $C_3$-SAM on ZnO is expected to tune the work function of the electrode surface due to the formation of the permanent dipole moment. First, we calculated the strength of the dipole moment of $C_3$-SAM on the ZnO surface by density functional theory (DFT) at the B3LYP/6-31G(d) level using the Gaussian 03 program[43] which had been successfully applied in previous studies.[44−46] The calculation indicated the bonding of $C_3$-SAM onto the ZnO surface would induce the dipole moment directing from the ZnO to perovskite with a strength of 3.14 debye. This dipole moment is expected to lower the work function of ZnO by bending the vacuum energy level. The UPS measurement (Figure 4b) showed that the work function of ZnO is appreciably lowered from 4.17 to 3.52 eV with deposition of $C_3$-SAM, which is more compatible with the CBM (−3.75 eV) of the $CH_3NH_3PbI_3$ perovskite (see Figure 1b). The lowered work function with $C_3$-SAM deposition would improve the energy level alignment and electronic coupling between the ZnO and perovskite, which increased the carrier extraction and charge generation. Also, the lowered cathode work function would provide a larger built-in potential to facilitate the charge transport. These effects would contribute to the increase in $J_{SC}$, FF, and $V_{OC}$ of PSC.[47]

**Reduced Trap States.** The charge traps were typically observed in perovskite film. Although these trap states were reported to be extremely shallow (~10 meV),[48] the reduction of the trap states was demonstrated to improve the PSC performance.[18] These trap states were discovered to be greatly related to the morphology of perovskite film,[21,22,49] e.g. crystallinity and grain size.[21,22,50] One of the methods to examine these trap states is the photoluminescence (PL) technique.[18] Here we studied the variation of the trap states with deposition of $C_3$-SAM by means of PL spectra. Figure 4c showed the steady state photoluminescence (ST-PL) spectra of perovskite films on bare ZnO and $C_3$-SAM modified ZnO, which were excited at 409 nm, and detected at the band edge of the $CH_3NH_3PbI_3$ perovskite films, e.g. from 700 to 850 nm. To eliminate the influence of exciton quenching induced by the ZnO, samples on silica with or without $C_3$-SAM modification were first examined. As shown in Figure 4c, compared with the perovskite on silica, the PL intensity of perovskite on $C_3$-SAM modified silica was significantly increased. The ST-PL intensity enhancement of perovskite film on silica with $C_3$-SAM deposition was attributed to the reduction of trap states mediated PL behavior, which was reported to be detrimental for light emission.[22] Therefore, it was clear that the deposition of $C_3$-SAM significantly reduced the number of trap states due to the improved morphology.

Similarly, the perovskite on $C_3$-SAM modified ZnO exhibited higher PL intensity than that without $C_3$-SAM, which reconfirms the reduction of trap states. The PL intensity of the $CH_3NH_3PbI_3$ perovskite film on the ZnO/$C_3$-SAM is significantly lower than that on the silica/$C_3$-SAM substrates, with nearly 85% of PL quenched. This was attributed to the electronic coupling between the ZnO and perovskite.[22] Interestingly, the PL intensity of the perovskite film on the $C_3$-SAM modified ZnO was even stronger than that on silica substrates, resulting from an interplay of reduction of trap states mediated PL and electronic coupling. In all, the enhanced PL intensity with deposition of $C_3$-SAM verified the reduction of trap state defects in the perovskite film. This would suppress the charge recombination and increase the exciton diffusion length for highly efficient PSC.

**Strengthened Electronic Coupling.** The excitonic relaxation dynamics of perovskite was demonstrated important in determining the device performance,[50] which was critically related to the morphology of the perovskite film[26] and the electronic coupling with the charge carrier quenching layer.[51] Faster charge transfer or stronger electronic coupling favored efficient charge generation and high PCE.[47] The transient PL spectra of perovskite crystalline film with deposition of $C_3$-SAM on ZnO were studied to have an insight into the carrier dynamics. As shown in Figure 4d, most excitons of the $CH_3NH_3PbI_3$ perovskite film on silica substrate showed an averaged lifetime of ~200 ns with nearly first order decay,[18,22,51] although a little shorter lifetime species were observed in the spectra. However, the carrier lifetime of $CH_3NH_3PbI_3$ perovskite film on either the ZnO or the $C_3$-SAM modified ZnO showed more complex charge dynamic processes, which could be classified into three species shown in Table 2. The decay component of $\tau_1$ ~2 ns might come from bimolecular recombination, and the decay component of $\tau_2$ ~20 ns could be attributed to recombination of free carriers in the radiative channel.[40] Owing to the strong electronic coupling between the $CH_3NH_3PbI_3$ and the ZnO film, the PL decay lifetime of perovskite on the ZnO with or without $C_3$-SAM is significantly reduced compared with that on the silica/$C_3$-SAM substrate. This is consistent with the PL quenching observed in the ST-PL spectra. Notably, the free carrier decay time of perovskite ($\tau_2$) on the $C_3$-SAM modified ZnO is appreciably shorter than that on the bare ZnO. The faster charge transfer rate indicated stronger electronic coupling between the ZnO


DOI: 10.1021/ja512518r
J. Am. Chem. Soc. 2015, 137, 2674−2679

and $CH_3NH_3PbI_3$ perovskite on $C_3$-SAM modified ZnO. This could be attributed to the more compatible energy level of ZnO with the CBM of $CH_3NH_3PbI_3$ film upon $C_3$-SAM deposition. Notably, although the $C_3$-SAM induced faster electron transfer favoring PL quenching, the deposition of $C_3$-SAM, on the other hand, led to trap-state reduction that should enhance the PL intensity. The interplay of these two factors resulted in the slightly increased PL intensity of perovskite on $C_3$-SAM modified ZnO, as compared to that on ZnO without SAM (Figure 4c).

In addition, the long lifetime PL species was observed in the perovskite film on ZnO with or without $C_3$-SAM modification. This could be attributed to the trap states mediated PL species. Through fitting the transient PL spectra to the empirical equation, we found that the number of the trap mediated PL is remarkably reduced with the deposition of $C_3$-SAM. Nearly 80% of the perovskite PL was emitted through the trap states on the bare ZnO, while this portion was reduced to 16% with insertion of $C_3$-SAM. This result suggested the reduced number of trap states with deposition of $C_3$-SAM, which was consistent with the ST-PL quenching discussed above.

## CONCLUSIONS

In conclusion, we have demonstrated a significant PCE improvement of $CH_3NH_3PbI_3$ perovskite solar cells from 11.96% (best) to 15.67% (best), as induced by inserting a self-assembling monolayer of 3-aminopropanoic acid between the ZnO and the perovskite. The deposition of the 3-amino-propanoic acid resulted in the improved morphology of the crystalline $CH_3NH_3PbI_3$ perovskite film, the increased light absorption of the perovskite film, the lowered cathode work function, and the enhanced electronic coupling between the ZnO layer and the perovskite film. All these factors contributed to the 31% surge in the PCE value. Our work highlights the effect of substrate properties on perovskite morphology control and its application in PSC as an efficient strategy to improve the device performance.

## ASSOCIATED CONTENT

### Supporting Information

Figure S1 showing the EQE spectra of perovskite solar cells with or without $C_3$-SAM modification. This material is available free of charge via the Internet at http://pubs.acs.org.

## AUTHOR INFORMATION

### Corresponding Authors

*hanying_li@zju.edu.cn
*hzchen@zju.edu.cn

### Notes

The authors declare no competing financial interests.

## ACKNOWLEDGMENTS

This work was supported by the Major State Basic Research Development Program (2014CB643503), the National Natural Science Foundation of China (Grants 91233114, 383 51261130582, 51473142, and 51222302), and the program for Innovative Research Team in University of Ministry of Education of China ( IRT13R54).

## REFERENCES

(1) McGehee, M. D. *Nat. Mater.* **2014**, *13*, 845.
(2) Green, M. A.; Ho-Baillie, A.; Snaith, H. J. *Nat. Photonics* **2014**, *8*, 506.
(3) Boix, P. P.; Nonomura, K.; Mathews, N.; Mhaisalkar, S. G. *Mater. Today* **2014**, *17*, 16.
(4) Gratzel, M. *Nat. Mater.* **2014**, *13*, 838.
(5) Yang, Z. S.; Yang, L. G.; Wu, G.; Wang, M.; Chen, H. Z. *Acta Chim. Sin. (Engl. Ed.)* **2011**, *69*, 627.
(6) Park, N.-G. *Mater. Today.* **2014**, *18*, 65.
(7) Lee, M. M.; Teuscher, J.; Miyasaka, T.; Murakami, T. N.; Snaith, H. J. *Science* **2012**, *338*, 643.
(8) Liu, D.; Kelly, T. L. *Nat. Photonics* **2014**, *8*, 133.
(9) Docampo, P.; Ball, J. M.; Darwich, M.; Eperon, G. E.; Snaith, H. J. *Nat. Commun.* **2013**, *4*, 2761.
(10) *Nat. Mater.* **2014**, *13*, 837.
(11) Kojima, A.; Teshima, K.; Shirai, Y.; Miyasaka, T. *J. Am. Chem. Soc.* **2009**, *131*, 6050.
(12) Liu, M.; Johnston, M. B.; Snaith, H. J. *Nature* **2013**, *501*, 395.
(13) Chen, C.-W.; Kang, H.-W.; Hsiao, S.-Y.; Yang, P.-F.; Chiang, K.-M.; Lin, H.-W. *Adv. Mater.* **2014**, *26*, 6647.
(14) Eperon, G. E.; Burlakov, V. M.; Docampo, P.; Goriely, A.; Snaith, H. J. *Adv. Funct. Mater.* **2014**, *24*, 151.
(15) Malinkiewicz, O.; Yella, A.; Lee, Y. H.; Espallargas, G. M.; Graetzel, M.; Nazeeruddin, M. K.; Bolink, H. J. *Nat. Photonics* **2014**, *8*, 128.
(16) Zhou, H.; Chen, Q.; Li, G.; Luo, S.; Song, T.-b.; Duan, H.-S.; Hong, Z.; You, J.; Liu, Y.; Yang, Y. *Science* **2014**, *345*, 542.
(17) Kim, J.; Kim, G.; Kim, T. K.; Kwon, S.; Back, H.; Lee, J.; Lee, S. H.; Kang, H.; Lee, K. *J. Mater. Chem. A* **2014**, *2*, 17291.
(18) Noel, N. K.; Abate, A.; Stranks, S. D.; Parrott, E. S.; Burlakov, V. M.; Goriely, A.; Snaith, H. J. *ACS Nano* **2014**, *8*, 9815.
(19) Han, G. S.; Chung, H. S.; Kim, B. J.; Kim, D. H.; Lee, J. W.; Swain, B. S.; Mahmood, K.; Yoo, J. S.; Park, N.-G.; Lee, J. H.; Jung, H. S. *J. Mater. Chem. A* **2015**, DOI: 10.1039/C4TA03684K.
(20) Conings, B.; Baeten, L.; De Dobbelaere, C.; D'Haen, J.; Manca, J.; Boyen, H.-G. *Adv. Mater.* **2014**, *26*, 2041.
(21) D'Innocenzo, V.; Grancini, G.; Alcocer, M. J. P.; Kandada, A. R. S.; Stranks, S. D.; Lee, M. M.; Lanzani, G.; Snaith, H. J.; Petrozza, A. *Nat. Commun.* **2014**, *5*, 3586.
(22) Xing, G.; Mathews, N.; Sun, S.; Lim, S. S.; Lam, Y. M.; Grätzel, M.; Mhaisalkar, S.; Sum, T. C. *Science* **2013**, *342*, 344.
(23) Jeng, J.-Y.; Chiang, Y.-F.; Lee, M.-H.; Peng, S.-R.; Guo, T.-F.; Chen, P.; Wen, T.-C. *Adv. Mater.* **2013**, *25*, 3727.
(24) Burschka, J.; Pellet, N.; Moon, S.-J.; Humphry-Baker, R.; Gao, P.; Nazeeruddin, M. K.; Gratzel, M. *Nature* **2013**, *499*, 316.
(25) Docampo, P.; Hanusch, F. C.; Stranks, S. D.; Döblinger, M.; Feckl, J. M.; Ehrensperger, M.; Minar, N. K.; Johnston, M. B.; Snaith, H. J.; Bein, T. *Adv. Energy Mater.* **2014**, DOI: 10.1002/aenm.201400355.
(26) Grancini, G.; Marras, S.; Prato, M.; Giannini, C.; Quarti, C.; De Angelis, F.; De Bastiani, M.; Eperon, G. E.; Snaith, H. J.; Manna, L.; Petrozza, A. *J. Phys. Chem. Lett.* **2014**, *5*, 3836.
(27) Wu, Y.; Islam, A.; Yang, X.; Qin, C.; Liu, J.; Zhang, K.; Peng, W.; Han, L. *Energy Environ. Sci.* **2014**, *7*, 2934.
(28) Liang, P.-W.; Liao, C.-Y.; Chueh, C.-C.; Zuo, F.; Williams, S. T.; Xin, X.-K.; Lin, J.; Jen, A. K. Y. *Adv. Mater.* **2014**, *26*, 3748.
(29) Zuo, C.; Ding, L. *Nanoscale* **2014**, *6*, 9935.
(30) Yu, H.; Wang, F.; Xie, F.; Li, W.; Chen, J.; Zhao, N. *Adv. Funct. Mater.* **2014**, *24*, 7102.
(31) Jeon, N. J.; Noh, J. H.; Kim, Y. C.; Yang, W. S.; Ryu, S.; Seok, S. I. *Nat. Mater.* **2014**, *13*, 897.
(32) Ren, Z.; Ng, A.; Shen, Q.; Gokkaya, H. C.; Wang, J.; Yang, L.; Yiu, W.-K.; Bai, G.; Djurišić, A. B.; Leung, W. W.-f.; Hao, J.; Chan, W. K.; Surya, C. *Sci. Rep.* **2014**, *4*, 6752.
(33) Seetharaman, M.; Nagarjuna, P.; Kumar, P. N.; Singh, S. P.; Deepa, M.; Namboothiry, M. A. G. *Phys. Chem. Chem. Phys.* **2014**, *16*, 24691.
(34) Ogomi, Y.; Morita, A.; Tsukamoto, S.; Saitho, T.; Shen, Q.; Toyoda, T.; Yoshino, K.; Pandey, S. S.; Ma, T.; Hayase, S. *J. Phys. Chem. C* **2014**, *118*, 16651.


DOI: 10.1021/ja512518r
J. Am. Chem. Soc. 2015, 137, 2674−2679

(35) Wang, L.; Fu, W.; Gu, Z.; Fan, C.; Yang, X.; Li, H.; Chen, H. *J. Mater. Chem. C* **2014**, *2*, 9087.
(36) Min, J.; Zhang, Z.-G.; Hou, Y.; Quiroz, C. O. R.; Przybilla, T.; Bronnbauer, C.; Guo, F.; Forberich, K.; Azimi, H.; Ameri, T.; Spiecker, E.; Li, Y.; Brabec, C. J. *Chem. Mater.* **2015**, *27*, 227.
(37) Yip, H.-L.; Hau, S. K.; Baek, N. S.; Ma, H.; Jen, A. K. Y. *Adv. Mater.* **2008**, *20*, 2376.
(38) Krüger, J.; Plass, R.; Cevey, L.; Piccirelli, M.; Grätzel, M.; Bach, U. *Appl. Phys. Lett.* **2001**, *79*, 2085.
(39) Zhao, Y.; Zhu, K. *J. Phys. Chem. C* **2014**, *118*, 9412.
(40) Chen, Q.; Zhou, H.; Song, T.-B.; Luo, S.; Hong, Z.; Duan, H.-S.; Dou, L.; Liu, Y.; Yang, Y. *Nano Lett.* **2014**, *14*, 4158.
(41) Dualeh, A.; Tétreault, N.; Moehl, T.; Gao, P.; Nazeeruddin, M. K.; Grätzel, M. *Adv. Funct. Mater.* **2014**, *24*, 3250.
(42) Supasai, T.; Rujisamphan, N.; Ullrich, K.; Chemseddine, A.; Dittrich, T. *Appl. Phys. Lett.* **2013**, *103*, 183906.
(43) Frisch, M. J.; Trucks, G. W.; Schlegel, H. B.; Scuseria, G. E.; Robb, M. A.; Cheeseman, J. R.; Montgomery Jr, J. A.; Vreven, T.; Kudin, K. N.; Burant, J. C.; Millam, J. M.; Iyengar, S. S.; Tomasi, J.; Barone, V.; Mennucci, B.; Cossi, M.; Scalmani, G.; Rega, N.; Petersson, G. A.; Nakatsuji, H.; Hada, M.; Ehara, M.; Toyota, K.; Fukuda, R.; Hasegawa, J.; Ishida, M.; Nakajima, T.; Honda, Y.; Kitao, O.; Nakai, H.; Klene, M.; Li, X.; Knox, J. E.; Hratchian, H. P.; Cross, J. B.; Bakken, V.; Adamo, C.; Jaramillo, J.; Gomperts, R.; Stratmann, R. E.; Yazyev, O.; Austin, A. J.; Cammi, R.; Pomelli, C.; Ochterski, J. W.; Ayala, P. Y.; Morokuma, K.; Voth, G. A.; Salvador, P.; Dannenberg, J. J.; Zakrzewski, V. G.; Dapprich, S.; Daniels, A. D.; Strain, M. C.; Farkas, O.; Malick, D. K.; Rabuck, A. D.; Raghavachari, K.; Foresman, J. B.; Ortiz, J. V.; Cui, Q.; Baboul, A. G.; Clifford, S.; Cioslowski, J.; Stefanov, B. B.; Liu, G.; Liashenko, A.; Piskorz, P.; Komaromi, I.; Martin, R. L.; Fox, D. J.; Keith, T.; Al-Laham, M. A.; Peng, C. Y.; Nanayakkara, A.; Challacombe, M.; Gill, P. M. W.; Johnson, B.; Chen, W.; Wong, M. W.; Gonzalez, C.; Pople, J. A. *Gaussian 03*; Gaussian Inc.: Wallingford, CT, 2004.
(44) Ling, J.; Liu, J.; Shen, Z.; Hogen-Esch, T. E. *J. Polym. Sci., Part A: Polym. Chem.* **2011**, *49*, 2081.
(45) Ling, J.; Huang, Y. *Macromol. Chem. Phys.* **2010**, *211*, 1708.
(46) Fu, W.; Wang, L.; Ling, J.; Li, H.; Shi, M.; Xue, J.; Chen, H. *Nanoscale* **2014**, *6*, 10545.
(47) Zhu, Z.; Ma, J.; Wang, Z.; Mu, C.; Fan, Z.; Du, L.; Bai, Y.; Fan, L.; Yan, H.; Phillips, D. L.; Yang, S. *J. Am. Chem. Soc.* **2014**, *136*, 3760.
(48) Oga, H.; Saeki, A.; Ogomi, Y.; Hayase, S.; Seki, S. *J. Am. Chem. Soc.* **2014**, *136*, 13818.
(49) Wu, K.; Bera, A.; Ma, C.; Du, Y.; Yang, Y.; Li, L.; Wu, T. *Phys. Chem. Chem. Phys.* **2014**, *16*, 22476.
(50) Wehrenfennig, C.; Liu, M.; Snaith, H. J.; Johnston, M. B.; Herz, L. M. *Energy Environ. Sci.* **2014**, *7*, 2269.
(51) Stranks, S. D.; Eperon, G. E.; Grancini, G.; Menelaou, C.; Alcocer, M. J. P.; Leijtens, T.; Herz, L. M.; Petrozza, A.; Snaith, H. J. *Science* **2013**, *342*, 341.


DOI: 10.1021/ja512518r
*J. Am. Chem. Soc.* 2015, 137, 2674−2679